ELSEVIER

Surface Science 492 (2001) 270–284

SURFACE SCIENCE

www.elsevier.com/locate/susc

Phonons of clean and metal-modified oxide films: an infrared and HREELS study

Martin Frank, Kai Wolter, Norbert Magg, Michael Heemeier, Ralf Kühnemuth [1], Marcus Bäumer, Hans-Joachim Freund *

Fritz-Haber-Institut der Max-Planck-Gesellschaft, Faradayweg 4-6, D-14195 Berlin, Germany

Received 5 May 2001; accepted for publication 27 July 2001

Dedicated to Prof. Dr. Henning Neddermeyer on the occasion of his 65th birthday

Abstract

Vibrational properties of thin dielectric films may be investigated by infrared spectroscopy and high-resolution electron-energy-loss spectroscopy (HREELS). Infrared absorption by dielectric films occurs near the frequencies of longitudinal optical bulk phonons (Berreman effect); electron energy losses due to Fuchs–Kliewer surface phonons are observed at similar energies. We report a comparative study of the phonon features of an ultra-thin, well-ordered aluminum oxide film on NiAl(1 1 0) by infrared reflection-absorption spectroscopy (IRAS) and HREELS. At least fourteen vibrational modes are identified. While the spectra are similar to those expected from macroscopic dielectric theory, a detailed band assignment will require microscopic lattice dynamical calculations. Metal particles are grown on the alumina film by vapor deposition of palladium, rhodium, iridium, vanadium, and aluminum. Their sizes, as determined by scanning tunneling microscopy (STM), range from few atoms up to several thousand atoms. Infrared spectroscopy serves to study the impact of the admetals on the oxide phonons. Detailed data on the damping, frequency shift, and broadening of the most intense oxide phonon as a function of metal exposure are presented, spanning an exposure range from below 0.01 to several monolayers. Pd induces a red-shift of the phonon mode, while Rh, Ir, V, and Al initially cause a blue-shift. At larger exposures, most metals induce a shift to lower frequencies. Adsorbed CO and ethene give rise to further changes of the phonon spectrum. Possible reasons for the observed behavior are discussed.

Keywords: Infrared absorption spectroscopy; Dielectric phenomena; Nucleation; Carbon monoxide; Ceramic thin films; Clusters; Insulating films; Metal–insulator interfaces

1. Introduction

Phonon spectra of many crystalline oxide films in vacuum have been studied by high-resolution electron-energy-loss spectroscopy (HREELS) [1,2]. By infrared spectroscopy, a much higher spectral resolution might be attained than that available in HREELS. To our knowledge, however, such

* Corresponding author. Tel.: +49-30-8413-4100; fax: +49-30-8413-4101.

E-mail address: freund@fhi-berlin.mpg.de (H.-J. Freund).

[1] Present address: Max-Planck-Institut für biophysikalische Chemie, Am Fassberg 11, D-37077 Göttingen, Germany.

0039-6028/01/$ - see front matter
PII: S0039-6028(01)01475-3

infrared studies are lacking. Only a single experiment performed under ambient conditions and thus ill-defined surface properties has been reported [3,4].

The use of infrared spectroscopy for the study of oxide films has mainly been driven by technological applications, focusing on amorphous or polycrystalline films. It enables the characterization of oxide scales on corroded metals and alloys with a thickness in the micrometer regime [5–7] as well as of nanometer-thick oxide films relevant as gate dielectrics in metal-oxide-semiconductor transistors [8,9]. Motivated by, e.g., their use in solar absorbers, also metal-oxide composites known as cermets have been studied by infrared spectroscopy [10–13].

Both thickness and composition of oxide films are accessible by monitoring the position and intensity of infrared features at the transverse optical (TO) and longitudinal optical (LO) phonon frequencies. In this, use is made of the Berreman effect: While in bulk dielectrics infrared absorption only occurs at the frequencies of their TO phonon modes, in transmission and reflection spectra of dielectric films taken with p-polarized light at an oblique angle, structures near the positions of the LO phonon modes are observed as well [14,15]. This phenomenon is due to surface charges generated by vibrations polarized normal to the surface [14]. For thick films, detailed connections between infrared optical properties and vibrational modes may be established in terms of macroscopic lattice dynamics and dielectric continuum theory [16,17]. Microscopic lattice dynamics shows that prominent features near the TO and LO frequencies still dominate the infrared spectra [17] (and electron-energy-loss spectra [18]) of slabs as thin as 1–2 nm.

Aside from the oxide film thickness [9,19,20], also metal inclusions [3,4,13] have occasionally been observed to influence the position of phonon infrared bands. However, this has not been studied in detail.

Similar observations of metal-induced phonon shifts were made in several HREELS studies of metal deposits on oxide surfaces [21–23] and thin films [24,25]. Such data should be comparable to infrared spectra, as HREELS in the dipole scattering regime is based on the same fundamental photon absorption mechanism as infrared spectroscopy [26]. For Pd/TiO_2 [23], Ag/MgO [25], Cu/ZnO [22], and Cu/MgO (where the Cu is oxidized to Cu_2O) [21], adlayer-induced red-shifts occurred, while for Ni/Al_2O_3 [24] two out of three phonon losses were blue-shifted. However, the limited spectral resolution in most such studies has precluded a precise quantification of the metal-induced shift as a function of metal load.

In view of the clear lack of infrared studies of ordered oxide films, we performed a detailed infrared reflection-adsorption spectroscopy (IRAS) study of a thin, well-ordered alumina film grown on a NiAl(1 1 0) surface under ultra-high vacuum (UHV) conditions. The infrared spectrum of the clean alumina film is compared to HREELS data of unprecedented quality. We then studied the influence of deposited metal particles on its infrared phonon spectrum utilizing vapor deposition of Pd, Rh, Ir, V, and Al, and varying the metal load across three orders of magnitude. The nucleation and growth behavior was controlled by scanning tunneling microscopy (STM). Additionally, we investigated changes due to molecular CO and ethene chemisorbed on the metal aggregates. The infrared measurements enable a detailed quantification of the damping, shifting and broadening of substrate phonons by the adlayers. Possible reasons for the observed behavior are discussed.

2. Experimental

STM and infrared experiments were performed in a single multi-chamber UHV system (except for the preparation and STM imaging of the Al deposit, which was performed in a second, similar UHV system). Its base pressure was below 2×10^{-10} mbar. The NiAl(1 1 0) crystal was mounted on a sample carrier which could be transferred between the various experimental stages. The crystal temperature was monitored by a NiCr/Ni thermocouple spot-welded to the sample.

STM images were taken with a variable temperature scanning tunneling microscope (Omicron). As the sample transfer system between the preparation and infrared stage on the one hand

and the microscope on the other hand was not equipped with sample cooling facilities, the microscope was also operated at room temperature. Infrared spectra were acquired with a vacuum infrared spectrometer (Bruker IFS 66v/S). A liquid nitrogen cooled MCT detector was used to detect the p-polarized light reflected from the sample surface at 84° grazing incidence. Its mid-infrared sensitivity range extends down to 600 cm^{-1}. Typically, 1024 scans were accumulated, corresponding to an accumulation time of 160 s. For the spectrum of the clean oxide film, 8192 scans were accumulated. The spectral resolution after apodization was 3.3 cm^{-1}. The sample temperature during measurement was 90 K, except for the V deposits prepared at 300 K, for which the reference and sample spectra were taken at 300 K.

HREEL spectra were recorded in a different UHV system equipped with a VSI Delta 0.5 instrument (resolution limit: 0.5 meV = 4 cm^{-1}). In this chamber, the crystal was spot-welded to two W rods. A NiCr/Ni thermocouple was used to monitor the crystal temperature. Data were taken in specular geometry with an energy resolution of 1.4 meV = 11 cm^{-1} at a primary energy of 5 eV and an average count rate of 1.2×10^5 counts/s in the elastic peak. The step width was 4 cm^{-1}. Spectra from eight different oxide preparations were added, resulting in a total accumulation time of 96 min. The sample temperature during measurement was 90 K.

The alumina film was prepared via oxidation of NiAl(1 1 0) [27]. After dosage of about 3000 L O_2 (1 L = 10^{-6} Torr s) onto the clean NiAl(1 1 0) single crystal surface at a sample temperature of 550 K, the crystal was briefly annealed to temperatures between 1100 and 1300 K. Usually, two oxidation/annealing cycles were employed to ensure complete oxidation of the surface. The oxide quality was checked by STM or by low-energy electron diffraction.

Pd (>99.95%), Rh (>99.9%), Ir (>99.9%), and V (>99.8%) were evaporated from a rod via electron bombardment. During evaporation the sample was put on a retarding potential to avoid effects due to metal ions accelerated towards the sample. Al (>99.999%) was evaporated from a resistively heated alumina crucible. Flux calibration was performed with a quartz crystal microbalance as well as by two-dimensional submonolayer growth on NiAl(1 1 0) and subsequent STM measurements. Deposition rates varied between 0.11 and 0.45 monolayers (ML) per min (1 ML Pd, Rh, Ir, V, and Al correspond to 1.53, 1.60, 1.57, 1.54, and 1.41×10^{15} atoms cm^{-2}, respectively). To minimize the time-dependent influence of background gases on metal nucleation and growth, and thus on the vibrational properties, for each amount of deposited metal studied the clean oxide surface was prepared afresh.

For the adsorption experiments, the samples were exposed to CO (AGA, >99.997%) or C_2H_4 (AGA, >99.95%), utilizing a pinhole doser. CO and ethene do not adsorb on the clean oxide film at 90 K or above [28,29].

3. Results and discussion

First, we present data on the clean alumina film. We then turn to the metal-modified surface and finally to the impact of molecular adsorbates. In each section, we first discuss structural evidence, followed by vibrational data.

3.1. Alumina film

An STM image of the alumina film grown on the NiAl(1 1 0) single crystal surface [27,30] is presented in Fig. 1. The film exhibits a high degree

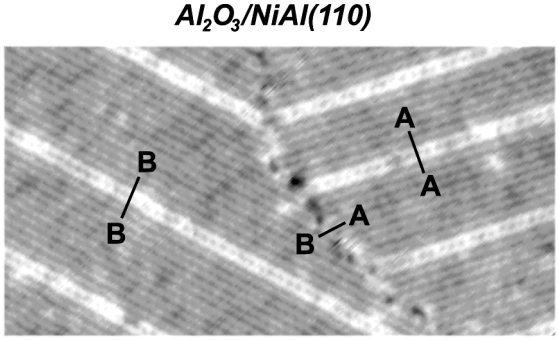

Fig. 1. STM image (775 Å × 400 Å) of the alumina film grown on NiAl(1 1 0). (A–A), (B–B): antiphase domain boundaries, (A–B): reflection domain boundary [31].

of order and is atomically flat [27,30] with a constant thickness of 5.6 Å [32], probably corresponding to two Al–O layers. It contains no Ni ions and is most likely oxygen terminated. Phonon spectra point to a structure similar to γ-Al_2O_3 [27,33–35] (see below). This is supported by transmission electron microscopy images [36]. The oxygen ions form a nearly hexagonal structure, which is slightly distorted as revealed by a large rectangular unit cell [27].

The film exhibits a characteristic defect structure [30,37], consisting of (a) a network of line defects, most notably antiphase domain boundaries with a characteristic distance of 100–200 Å (Fig. 1, A–A and B–B), but also reflection domain boundaries (Fig. 1, A–B) and substrate steps, and (b) point defects with a number density of about 1×10^{13} cm^{-2}.

In HREELS observations of the alumina film on NiAl(1 1 0), so far performed at a spectral resolution between 25 and 70 cm^{-1}, three single loss peaks at 400–425 cm^{-1} (ν_1), at 620–635 cm^{-1} (ν_2), and—most intense—at 870–880 cm^{-1} (ν_3) were identified [1,27,33–35]. [2] Based on a comparison with loss spectra simulated within the framework of dielectric theory, a film structure similar to γ-Al_2O_3 was clearly favored over an α-Al_2O_3-like structure [1,27,34]. For γ-Al_2O_3, the predicted energies are 403, 669, and 917 cm^{-1} [1]. The failure to observe a fourth mode, expected around 783 cm^{-1} [1], may have been due to its very low predicted intensity. It was pointed out [34] that for the determination of exact alumina film structures more refined optical data would be required, as almost the same three-phonon spectra are expected for various transition-phase Al_2O_3 films. A structurally well-characterized θ-Al_2O_3 film [38], being close in crystal structure to γ-Al_2O_3, indeed exhibits a similar loss spectrum as our film [1]. The presence of a transition-phase Al_2O_3 on NiAl(1 1 0) is thus firmly established.

Relying on a macroscopic picture, the loss peaks have been attributed to Fuchs–Kliewer phonons [1,27,33]. Such macroscopic surface modes arise at the surface of a dielectric half-space or slab [17,39,40]. For a dielectric slab on top of a metallic substrate, Fuchs–Kliewer loss signals near the LO frequencies of the corresponding bulk dielectric are expected [39]. This phenomenon is analogous to the Berreman effect in infrared spectroscopy [14,15], i.e. the observation of structures near the positions of the LO phonon modes in spectra of dielectric films taken at an oblique angle. An important difference between the observation of Fuchs–Kliewer phonons by HREELS and the Berreman effect in infrared spectroscopy arises from different extents of momentum transfer. In photon absorption, momentum transfer is very small. The band structure is thus probed in a region where surface lattice vibrations and electromagnetic fields are strongly coupled, i.e. in the regime of surface phonon–polaritons [16,17]. By contrast, at the much larger momentum transfers typical for electron scattering a pure phonon picture is sufficient. Despite these differences, features at similar energies are expected.

This is indeed the case for the thin alumina film under consideration, as illustrated by Fig. 2. In infrared spectra and in very highly resolved HREEL spectra (11 cm^{-1}), both acquired at 90 K, the most intense structures are located near 420, 620–660, and 860–870 cm^{-1}. This is fully consistent with data reported previously [1,27,33–35]. Additionally, our spectra reveal a wealth of new information on the oxide phonons. In the infrared spectrum (Fig. 2a), the most intense band ν_3 is located at 871 cm^{-1}, possessing a remarkably low halfwidth of 11–12 cm^{-1} (at 300 K, its position and width are 866 and 16 cm^{-1}, respectively). The ν_2 mode is resolved into two narrow signals of similar intensity at 622 and 660 cm^{-1}. Weak features at 718 cm^{-1}, at about 851 cm^{-1} (in the low-energy tail of the ν_3 mode) and at 954 cm^{-1} are newly identified. We also succeeded to identify most of these features by HREELS (Fig. 2b). A tail at about 805 cm^{-1} found by HREELS might also be present in the infrared spectrum; baseline instabilities, however, have not allowed an unambiguous identification. At lower loss energies, many new signals are identified. A loss feature from the clean

[2] Note that the spectrum shown in Ref. [27] was recorded after oxidation with ^{18}O. Corresponding ^{16}O data are reported in Ref. [33].

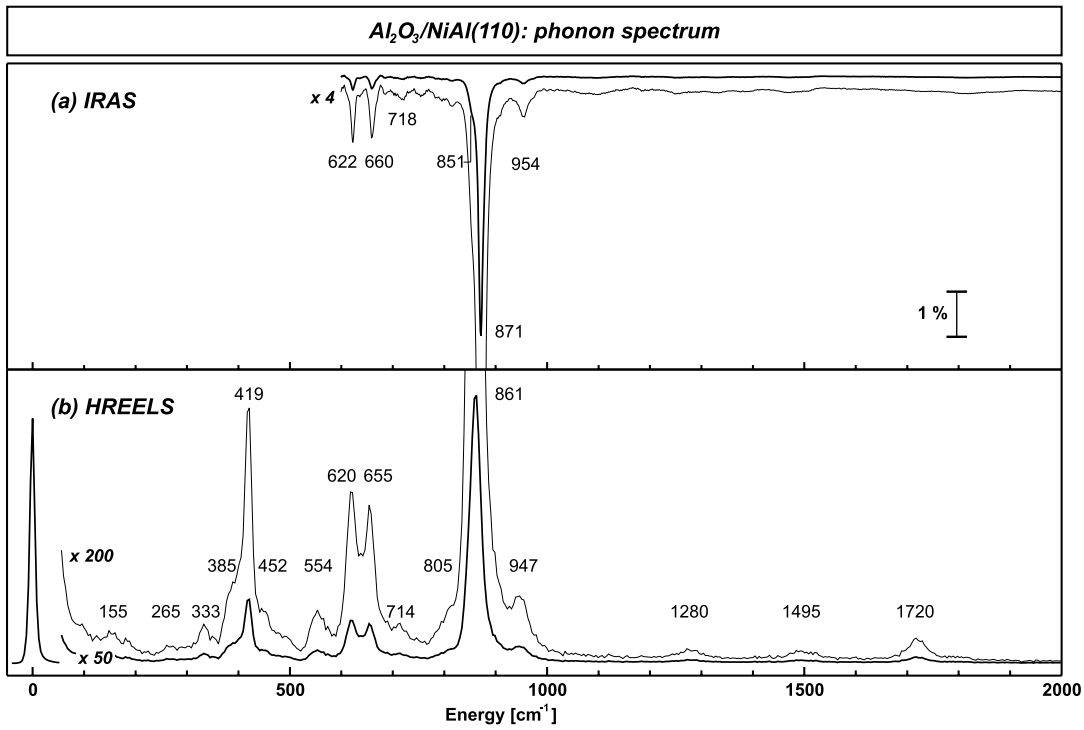

Fig. 2. (a) Infrared and (b) HREEL spectra of the alumina film recorded at 90 K.

NiAl(1 1 0) surface at 220 cm^{-1} (not shown) has disappeared upon oxidation.

Altogether, at least 14 signals are reproducibly observed at energies below 1000 cm^{-1}. Their energies and those of three multiple loss features at higher energies are listed in Table 1.

While the gross spectral behavior of the alumina film is similar to that predicted by macroscopic dielectric theory, its newly identified phonon bands do not fit into this picture. Bulk γ-Al_2O_3 possesses four infrared active vibrational modes, so four thin film modes near the LO frequencies of bulk γ-Al_2O_3 are expected as well [41]. By contrast, at least 14 phonon modes are observed. Relying on macroscopic dielectric theory, this points to a deviating film structure. Indeed, based on the large size of its unit cell, a distorted structure was postulated for the film [27]. It should be kept in mind, however, that even if the film is very similar to γ-Al_2O_3, the overall success in modeling the vibrational behavior of a stack of two atomic double layers by a macroscopic theory

Table 1
HREELS loss energies and infrared absorption frequencies (cm^{-1}) observed from the thin alumina film on NiAl(1 1 0) at 90 K. The frequencies of the most prominent signals corresponding to the loss features v_1, v_2, and v_3 reported previously [1,27,33–35] are underlined

	HREELS	IRAS
Single losses	~155	–
	~265	–
	333	–
	~385	–
	419	–
	~452	–
	554	–
	620	622
	655	660
	714	718
	~805	?
	–	~851
	861	871
	947	954
Combination losses	1280	–
	1495	–
	1720	–

is surprising. While bulk features still contribute most to the infrared spectra at a thickness of 15 layers [17], in thinner films characteristic microscopic modes may be expected to dominate. The clear distinction between microscopic modes and Fuchs–Kliewer phonons possible for thicker slabs must therefore break down in the present case. A detailed understanding of the observed phonon features requires microscopic lattice dynamical models [17].

In earlier studies, microscopic assignments of the intense HREELS loss features v_1, v_2, and v_3 were indeed attempted. A lattice dynamical calculation for oxygen-terminated Al_2O_3 on Al(1 1 1), containing only two O layers just as our film, pointed to out-of-phase modes between the surface and the subsurface Al–O layer (v_1), between the surface Al and O planes (v_2) and between the subsurface Al and O planes (v_3) [42]. A different proposal, from an experimental study of both thin and thick alumina films, assigned the features to stretching vibrations of neighboring Al–O planes (v_1), to a group of stretching vibrations between tetrahedrally coordinated Al cations and their four nearest O neighbors (v_2), and to a group of stretching vibrations between octahedrally coordinated Al cations and their six nearest O neighbors (v_3) [34,35]. The latter authors pointed out that for γ-Al_2O_3 two slightly different sets of Al–O bonds exist in the tetrahedron geometry and three in the octahedron geometry. According to their assignment, a splitting of the v_2 feature into two and of the v_3 feature into three bands might therefore be expected [34,35]. While we indeed observe two bands of similar intensity near v_2, only one intense band dominates at v_3. However, this is not necessarily incompatible, as the vibrational dynamic dipole moments and thus the band intensities are not predicted. More detailed calculations will be required for a reliable structural assignment.

3.2. Metal deposits

The STM images in Fig. 3 illustrate the metal nucleation and growth behavior on the alumina film for Pd, Rh, and Ir at 90 K (top) and for Pd, Rh, Ir, V, and Al at 300 K (bottom). When deposited at room temperature, Pd and Rh nucleate at oxide line defects. All other deposits are

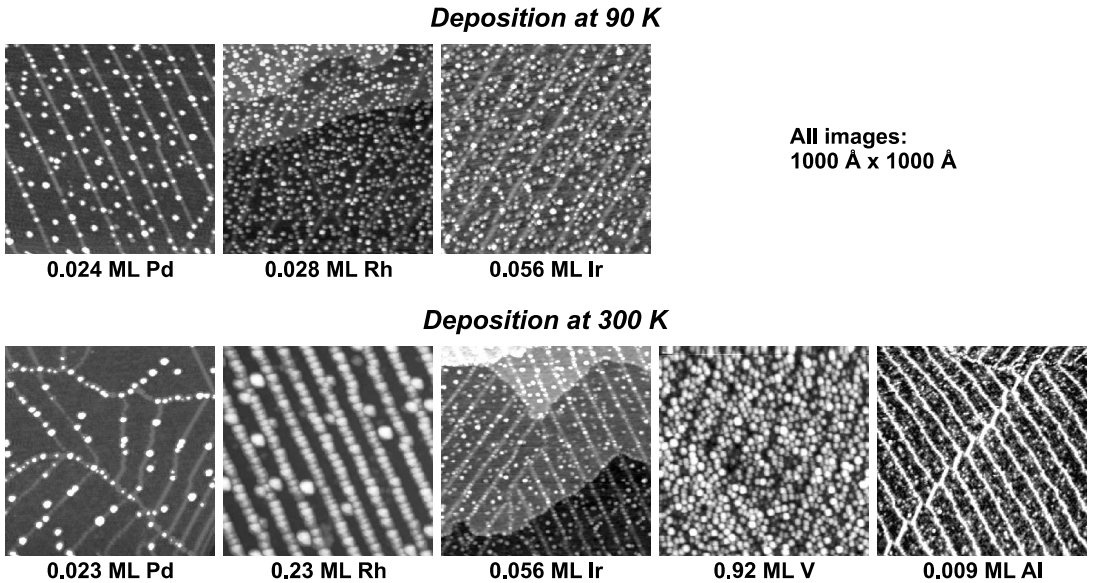

Fig. 3. Room-temperature STM images (1000 Å × 1000 Å) recorded after deposition of submonolayer metal exposures onto the thin alumina film: Pd, Rh, and Ir deposited at 90 K (top) and Pd, Rh, Ir, V, and Al deposited at 300 K (bottom). The line protrusions are domain boundaries of the oxide film.

distributed nearly isotropically, nucleating also within the oxide domains. Three-dimensional particles are formed in all cases [43].

In conjunction with our previous work on nucleation and growth on the alumina film [37,43–45], three types of metal nucleation site may be distinguished: (a) the oxide line defects, constituting the deepest potential wells for metal adatoms (Pd and Rh at 300 K), (b) point defects (Pd and Rh at 90 K; Ir, V, and possibly Al, at 300 K), and (c) surface sites between the point defects, possibly regular oxide sites, exerting the weakest influence on the metal atoms (Ir at 90 K). In the exposure regime studied, from 0.006 up to 6 ML, this nucleation behavior renders average particle sizes between few atoms and several thousand atoms accessible [37,43–45].

Metal nucleation is determined by the relation between the thermal energy of diffusing adatoms and the metal–oxide interaction strength at possible nucleation sites. The lower the substrate temperature, and the stronger the metal–oxide interaction, the more nuclei are formed. For the metals under consideration in the present study, the tendency to form a large number of nuclei rises according to $Pd < Rh < Ir \approx V \leqslant Al$ [37,43,44]. This order roughly correlates with a rising reactivity, as, e.g., given by their heats of oxide formation [46] (per mole of oxygen [47]). Under the experimental conditions employed in the phonon studies discussed below, we have indications that submonolayer amounts of V and Al are partially oxidized [43].

We now turn to the impact of the metal deposits onto the oxide vibrations. Fig. 4a shows a series of infrared spectra of the oxide film in the region of its most intense phonon mode ν_3 for the clean film (bottom) and for increasing Rh exposures at 90 K. The signal initially at 871 cm^{-1} first moves to higher wavenumbers by about 1 cm^{-1}, then to

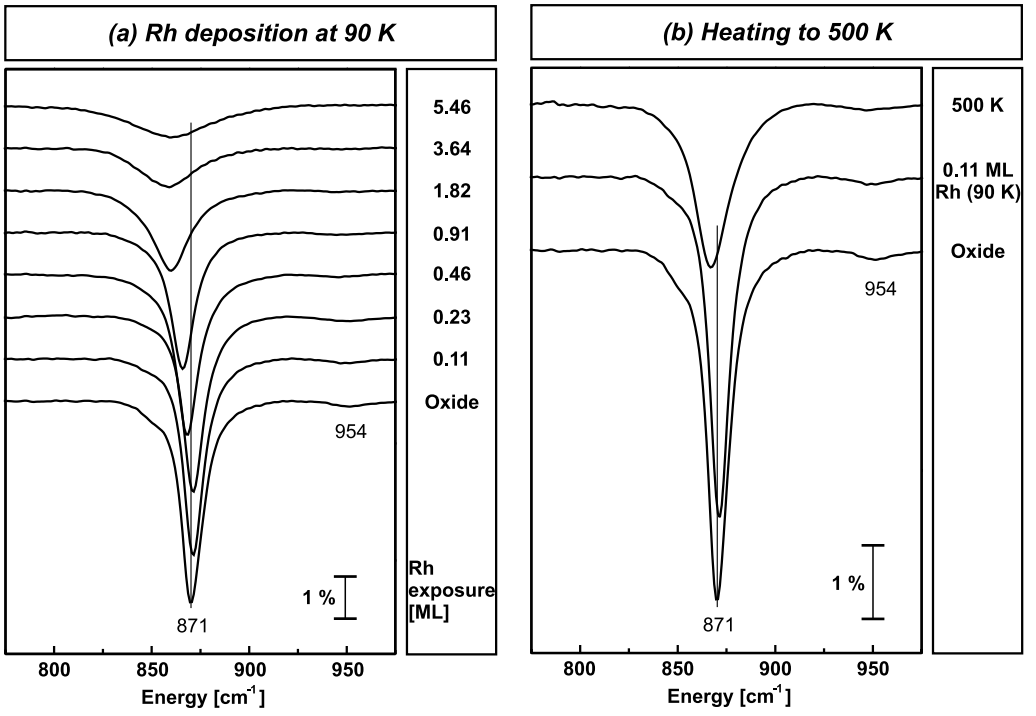

Fig. 4. (a) Infrared spectra of the alumina film in the region of its most intense phonon mode ν_3 for the clean film (bottom) and after exposing the film to increasing amounts of Rh at 90 K. (b) Infrared spectra of the alumina film in the region of its most intense phonon mode ν_3 for the clean film (bottom), after exposing the film to 0.11 ML Rh at 90 K (center) and after subsequent annealing to 500 K (top). All spectra were recorded at 90 K.

lower wavenumbers by up to 10 cm^{-1}. Concomitantly, it is damped and broadened. The weak signal at 954 cm^{-1} (Fig. 4a) and the ν_2 bands at 622 and 660 cm^{-1} (not shown) also disappear upon metal deposition. The overlap of the former signal with the high-frequency tail of ν_3 and the comparatively high noise level in the region near 635 cm^{-1} preclude a reliable quantification of intensities and positions already at intermediate metal exposures. However, the signal at 954 cm^{-1} appears to be attenuated somewhat faster than the other features. For the bands at 954 and 660 cm^{-1}, the data indicate small shifts to lower frequencies, while the position of the signal at 622 cm^{-1} seems to remain unaffected.

Heating a low Rh exposure to 500 K has similar consequences as a higher metal load: a damping, a shift, and a broadening of the mode ν_3 (Fig. 4b). Morphological changes by such a thermal treatment are small [43]. The particle number density stays nearly constant, only single Rh atoms diffuse to larger aggregates [48]. Minute modifications at the metal–oxide interface, such as a thermally induced rearrangement of interface Rh atoms into energetically more favorable sites, must therefore be responsible for the observed spectral changes. At the *surface* of the Rh particles, a local ordering process upon heating to 500 K has in fact been detected [48].

Series of infrared spectra for increasing metal exposures were recorded for Rh, Pd, and Ir deposited at 90 K and for Rh, Pd, Ir, V, and Al deposited at 300 K. In Fig. 5, characteristic parameters of the most intense oxide phonon mode ν_3—its integrated intensity and its position relative to those of the clean oxide film, and its halfwidth—are plotted as a function of metal exposure for metals deposited at 90 K (top) and at 300 K

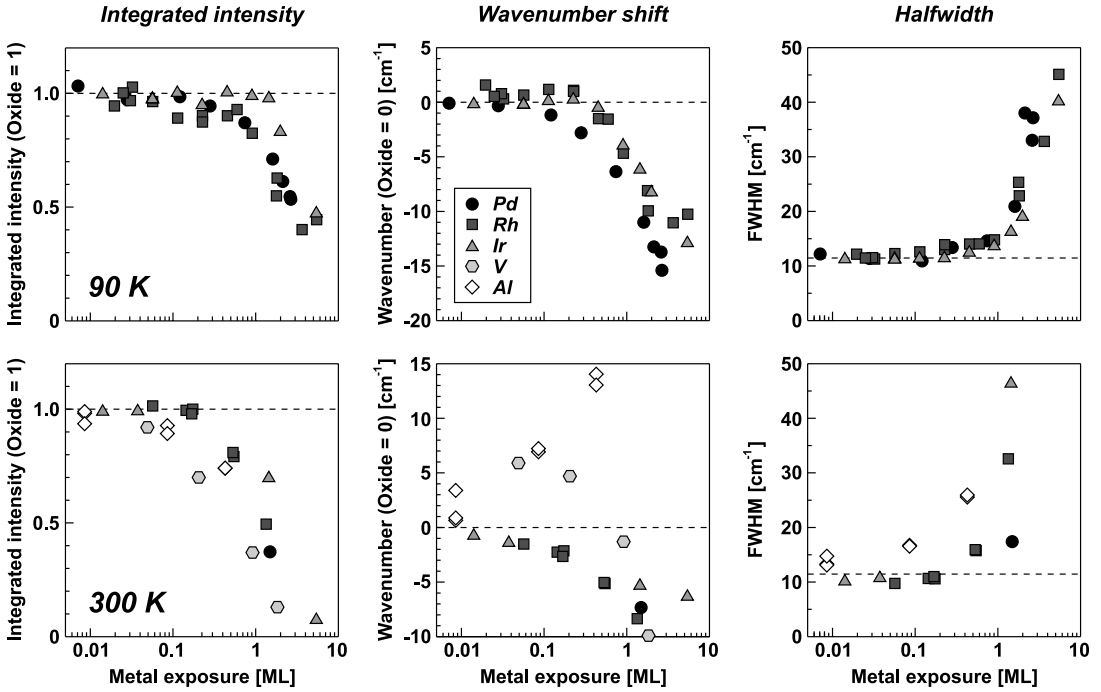

Fig. 5. Integrated intensity relative to the clean oxide film, wavenumber shift relative to the clean oxide film, and halfwidth (FWHM, full width at half maximum) of the most intense alumina infrared band ν_3 as a function of metal exposure. Top: Pd, Rh, and Ir deposited at 90 K. Bottom: Pd, Rh, Ir, V, and Al deposited at 300 K. All spectra were recorded at 90 K, except for those for V deposited at 300 K, which were recorded at 300 K. Due to their limited comparability, the halfwidths for V deposited at 300 K are omitted.

(bottom). [3] To render effects in all exposure regimes between 0.006 and 6 ML equally visible, a semi-logarithmic plot was chosen. Data at even larger Rh coverages were also taken. However, for these films, which are presumably closed, the attenuation and broadening is too strong to allow a reliable determination of the characteristic phonon parameters.

First, we turn to the integrated *intensity* of the ν_3 band (Fig. 5, left). All metals attenuate the phonon in a qualitatively similar way. There are, however, notable differences: At 90 K, the band intensity diminishes linearly with rising Pd or Rh exposure up to coverages of about 3 ML, as a linear plot clearly reveals; for Ir, by contrast, the intensity remains constant up to an exposure of 1.5 ML and only then drops to values similar to those of Rh and Pd deposits. The attenuation by Al and V, at 300 K, proceeds slightly faster than that by Pd, Rh, and Ir. Taking into account all available data, the influence of the five metals under consideration appears to increase according to $\mathrm{Ir} < \mathrm{Pd} \approx \mathrm{Rh} < \mathrm{Al} < \mathrm{V}$.

Concerning the *phonon frequency* (Fig. 5, center), differences between the metals are much more dramatic. Pd induces a red-shift which, at 90 K, is roughly proportional to the metal exposure up to a coverage of about 2 ML. Rh and Ir show the same behavior, after a tiny initial wave number increase in the 90 K case. For V deposited at 300 K, a very clear cross-over from blue-shift to red-shift at an exposure of about 1 ML is observed. Finally, Al deposition increases the phonon frequency in the whole coverage regime studied. In the low-coverage regime, the phonon frequency at a given metal exposure rises according to $\mathrm{Pd} < \mathrm{Ir} \leqslant \mathrm{Rh} < \mathrm{V} \approx \mathrm{Al}$. At large exposures, all metals (except, possibly, for Al) induce a red-shift of the oxide phonon.

The *phonon halfwidth* (Fig. 5, right) increases in all cases, the impact of Al being larger than that of Pd, Rh, and Ir.

We would like to start the discussion by listing phenomena which may be responsible for spectral changes such as the ones described above. First, we focus on macroscopic effects and on metal–oxide interaction phenomena not requiring intimate contact between overlayer and substrate:

– The *response of metal conduction electrons to the incoming infrared light* modifies the electromagnetic field transmitted to the dielectric and thus the spectral behavior of the surface. Percolated or closed metallic overlayers may exhibit a substantial infrared absorptance [49] and reflectance [50] already at a thickness of few nanometers, thereby efficiently screening the substrate. This leads to a vanishing infrared absorption in the oxide layer, i.e. an attenuation of its phonon modes [50]. A simple description of such phenomena may be based on the macroscopic dielectric properties of the substances involved. Indeed, the infrared properties of metal-oxide composites in the phonon region have been qualitatively modeled by effective-medium theories deriving a dielectric function of a mixed medium from those of its constituents [10–13]. Size-dependent electronic properties of small particles or thin films [49], or even the atomic nature of matter, are neglected in this way.

– The absorption cross-section for the excitation of lattice vibrations by infrared light is governed by the vibrational dynamic dipole moment of the absorber. If a dielectric substrate is covered by a metallic overlayer, the dynamic dipoles of its phonon modes will induce *image dipoles* in the metal conduction electron gas. This screening changes their absorption cross-section. Several authors [23,51–53] have held this type of dielectric screening responsible for intensity changes of Fuchs–Kliewer phonon losses in HREELS by metal deposits on oxide surfaces [21–23,51,54–56], oxide films [25,57–60], and semiconductor substrates [52,53]. Closed metal films [52,59,60] attenuate the substrate modes much more efficiently than three-dimensional aggregates [22,23,25]. Adsorbed gases, reducing the metallic character of the metal film, may reverse an admetal-induced damping [55,59], supporting a dielectric picture.

– Image dipoles may also affect band positions and halfwidths. As is well-known from molecular adsorbates on metal surfaces [61], the coupling of the vibrational dipole with its own image induces a

[3] The halfwidths after V deposition are omitted, as these data were determined at 300 K and may therefore not be directly comparable to the other data.

red-shift. Scattering of conduction electrons screening a vibrating dipole might reduce its lifetime and thus raise the absorption halfwidth.

– The oxide phonons could couple with *phonon modes of the metal*, leading to a frequency shift and broadening. However, metal phonons lie substantially lower in energy than the alumina phonon ν_3 under discussion [62] and multiphonon processes are improbable. Significant effects due to such a coupling are therefore unlikely in the present case.

Metal–substrate interactions operative at much shorter distances may be relevant as well. Such effects have been invoked to explain, e.g., different impacts of a deposit onto microscopic surface and subsurface oxide vibrations, respectively, as observed by HREELS [24,57]:

– A *mass* attached to a vibrating system, such as metal on a dielectric surface, may cause a detuning of the vibration.

– If a molecule vibrates close to a metal surface, it experiences a "wall effect" [63] due to the *Pauli repulsion* between its own electrons and those of the metal, causing a blue-shift. This may also be expected to occur for a dielectric film covered by a metal layer.

– *Chemical interactions*, i.e. changes in chemical bonding, at the interface may modify the vibrational properties of the system. Even slight induced anharmonicities of the oxide ion potentials may cause coupling between different substrate phonons, leading to frequency shifts and changes in halfwidth. Also charge flow between different orbitals during a vibrational period may have to be considered.

– The metal influences the *degree of surface order*, giving rise to phonon-defect scattering. Most notably, thermally induced metal diffusion through an oxide film has been shown to diminish its phonon intensities [24]. However, even metal particles on top of a structurally and chemically unaffected oxide introduce spatial heterogeneity into the system which might lead to a broadening of phonon bands.

– Oxide vibrations interacting with the metal electron gas may induce electron–phonon scattering. This reduces phonon lifetimes and thus broadens the corresponding absorption bands.

Concerning our infrared data for metal deposits on Al_2O_3/NiAl(1 1 0), an attempt to provide a full explanation based on a purely macroscopic phenomenon must fail. This follows from the observation of a substantial thermally induced damping, frequency shift, and broadening of the ν_3 mode (Fig. 4b), despite negligible morphological changes of the Rh deposit. This shows that atomic details of the metal–oxide interface are relevant. At large metal exposures, on the other hand, dielectric considerations certainly play an important part. To judge which properties of the admetals are responsible for the observed behavior, we shall now discuss our exposure-dependent data (Fig. 5) in more detail. We first take a closer look at the phonon intensity and then move on to its frequency and its halfwidth.

Most deposits reduce the *phonon intensity* (Fig. 5, left) already at intermediate exposures. We note that Pd and Rh at 90 and 300 K, and Ir at 300 K, nucleate at oxide point or line defects; at an exposure of 1.5 ML this results in particles consisting of 170 up to 3000 atoms [37,44] which are certainly metallic. In contrast with these deposits, 1.5 ML Ir grown at 90 K leave the phonon intensity unaffected. This correlates with the nucleation behavior: As Ir nucleates between the point defects at 90 K, smaller aggregates are formed. Such a deposit will have a reduced metallic screening capability. For Pd, Rh, and Ir, our observations therefore indicate a metallic screening mechanism at intermediate to high metal exposures.

V and Al cause a somewhat faster initial attenuation than Pd, Rh, and Ir. Judged by their heats of oxide formation [46] per mole of oxygen [47], V and Al are also by far the most reactive metals. Indeed, submonolayer amounts of V and Al on our alumina support are partially oxidized [43]. It is thus likely that their stronger influence on the phonon intensity at low exposures is due to a chemical perturbation of the oxide film.

The *phonon frequency* (Fig. 5, center) in the low-exposure regime (around 0.1 ML) is reduced only by Pd. The frequency is slightly increased by Ir and Rh, while V and Al lead to pronounced blue-shifts (see lower center panel). The phonon frequency thus rises according to $\mathrm{Pd} < \mathrm{Ir} \leqslant \mathrm{Rh} < \mathrm{V} \approx \mathrm{Al}$. This roughly correlates both with a decreasing d

orbital or d band population of these elements [64], consistent with dielectric phenomena, and with a rising reactivity [46], which would indicate chemical effects. We note that previous HREELS observations of oxide phonon energies at low metal coverages best support the second correlation [46]: Pd appeared to induce a downshift [23], with Cu the frequency initially remained constant [22], for Ni an upshift of two phonon bands was found (at an uncalibrated but supposedly low Ni exposure) [24]. From our observations, a dominant contribution to the frequency shift by mechanical detuning can be ruled out: Ir has by far the highest atomic mass of all elements considered, while it induces shifts similar to those of Pd and Rh.

At higher exposures (around 1 ML), a crossover from a blue-shift to a red-shift by Rh, Ir, and V occurs. This indicates that a different phenomenon now dominates the spectral behavior. For Al, there are no data available. Red-shifts were also observed previously by HREELS for Pd [23], Ag [25], and Cu [22]; only Ni [24] induced a blue-shift. A metallic character of the adlayer seems not to be required for the red-shift at intermediate coverages, as a significant shift to lower frequencies after deposition of 1.5 ML Ir at 90 K shows.

At 90 K, the *phonon halfwidth* (Fig. 5, right) increases similarly upon deposition of Pd, Rh, and Ir. Substantial broadening occurs at exposures above 1 ML. At 300 K, the halfwidth increases according to Pd < Rh < Ir. For these metals, the particle number density, and thus also the fraction of the surface covered by metal, increases in the same order. Al exhibits a nucleation behavior similar to that of Ir and induces a rapid broadening, too. It therefore seems that the extent of broadening is related to the metal–oxide contact area, pointing to phonon-defect scattering. Again, microscopic properties of the interface play a part: A small number of Rh particles prepared at room temperature lead to a stronger broadening than a low-temperature deposit forming more nuclei. A reduced phonon lifetime due to electron–phonon scattering is probably not the cause of the observed broadening: The halfwidth would then be expected to rise with rising density of states near the Fermi level; this quantity increases according to Al < Ir < Rh < Pd [64], which is not the order we observe.

3.3. Adsorbates

Adsorbed molecules on the metal particles may be used to modify the properties of the metals and to correlate this with changes in the phonon spectra. Concerning morphology, CO and ethene leave the metal aggregates unaffected in the pressure regime employed in this study. While electron diffraction pointed to a spreading of the Rh particles upon CO adsorption [65], this was not confirmed by our later studies [37]. However, chemisorption will change the electronic structure of the metal particles.

Series of phonon spectra for increasing metal exposures were recorded for metals deposited at 90 K and then gas-saturated at the same temperature. We studied CO-saturated Rh, Pd, and Ir particles and ethene-saturated Pd particles. In Fig. 6, the characteristic parameters of the most intense oxide phonon mode ν_3 are plotted (shaded symbols) as a function of metal exposure for CO adsorption (top) and for ethene adsorption (bottom). The data of the clean deposits are given for comparison (white symbols). For clarity, the gas-induced changes in intensity, wavenumber, and halfwidth with respect to the metal-modified surface are given in Fig. 7 (CO: shaded symbols; ethene: white symbols).

The following trends are identified: The *phonon intensity* (Figs. 6 and 7, left) increases upon gas saturation. At very low Rh and Ir exposures (below about 0.04 and 0.1 ML, respectively), CO slightly raises the *phonon frequency* (Figs. 6 and 7, center), while at higher exposures a red-shift relative to the pure metal deposit occurs. For CO on Rh, this shift reaches $-5\ \mathrm{cm}^{-1}$. By contrast, ethene on Pd induces a blue-shift compared to the clean metal particles. Concerning the *phonon halfwidth* (Figs. 6 and 7, right), for CO adsorption no clear trend is established. Ethene on Pd leads to a narrowing relative to the clean metal deposit.

In our discussion of the clean metal deposits (Section 3.2), two properties of the adlayer were identified as possible parameters governing the *phonon intensity* : its reactivity, mainly at low metal

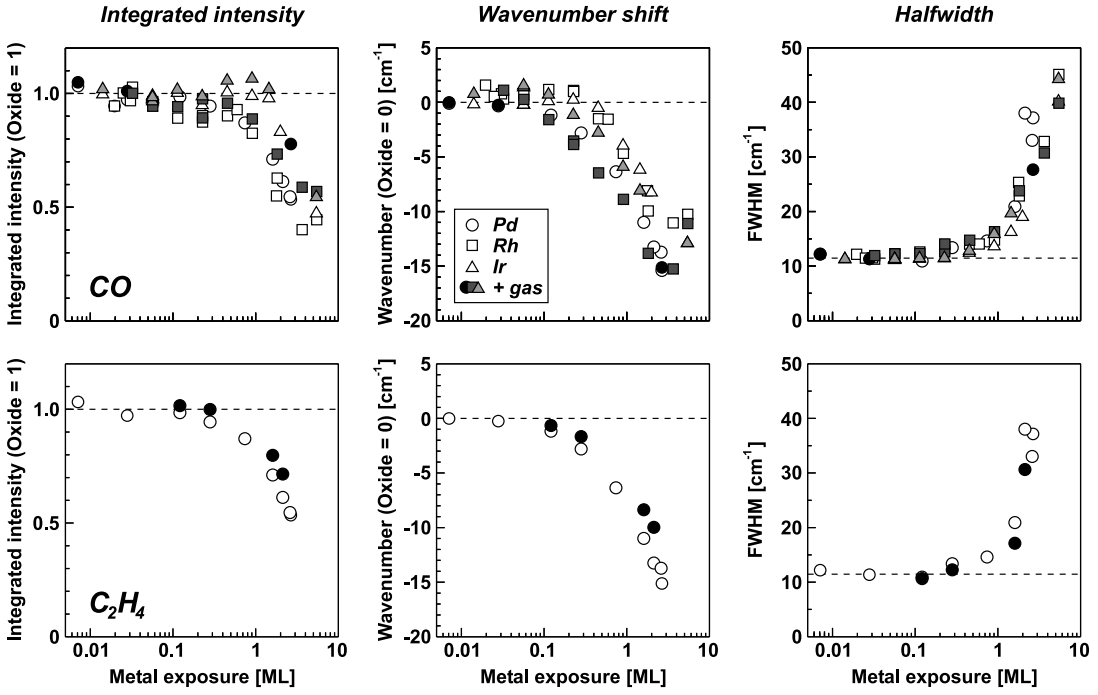

Fig. 6. Integrated intensity relative to the clean oxide film, wavenumber shift relative to the clean oxide film, and halfwidth of the alumina infrared band ν_3 as a function of metal exposure after metal deposition at 90 K (white symbols) and after gas saturation at the same temperature (shaded symbols). Top: CO adsorption on Pd, Rh, and Ir deposits. Bottom: ethene adsorption on Pd deposits.

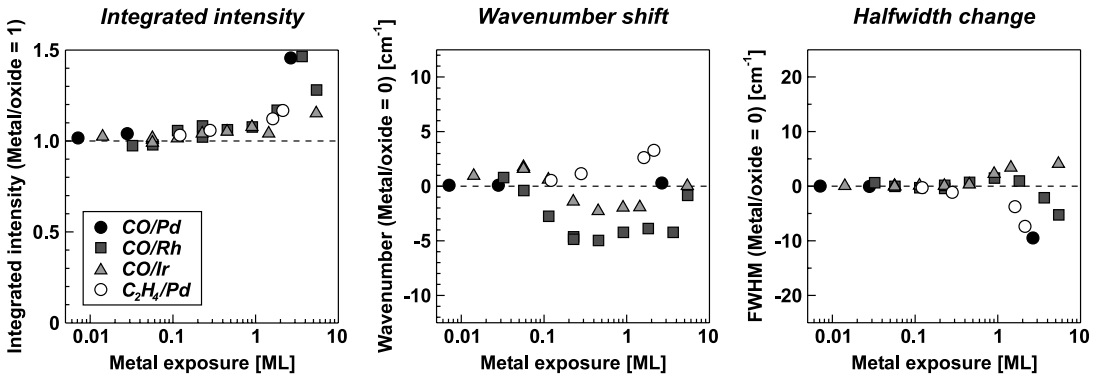

Fig. 7. Gas-induced change in integrated intensity, wavenumber, and halfwidth of the alumina infrared band ν_3 relative to the metal-modified oxide film as a function of metal exposure. Shaded symbols: CO adsorption on Pd, Rh, and Ir deposits. White symbols: ethene adsorption on Pd deposits.

exposures, and its metallicity. The partial lifting of the damping by CO and ethene (Figs. 6 and 7, left) might be related to either cause. For small particles, the metal–oxide interaction strength may be weakened by the chemisorbates due to bond order conservation. According to our correlation between reactivity and intensity, an increase in phonon intensity is then expected. At larger metal

exposures a dielectric phenomenon is more likely: adsorbed CO draws electrons from most transition metals [66] and localizes metal electrons in forming a chemical bond. This reduces the number of conduction electrons and thus metallic screening. Such a metal-to-nonmetal transition of Na/Cr_2O_3 was invoked previously to explain adsorbate-induced phonon intensity changes observed by HREELS [59]. On our thin alumina film, ethene transfers net charge into the Pd particles [29]. However, electron localization may still occur.

Taking into account the electron withdrawal by CO, the blue-shift found for the smallest Rh and Ir particles (Figs. 6 and 7, center) supports our correlation between a decreasing number of d electrons in the adlayer and a rising *phonon frequency*. The data at higher coverages and the *halfwidth* data are not easily rationalized by simple models.

4. Summary and conclusion

Utilizing infrared and HREEL spectroscopy, we have recorded the phonon spectrum of a thin alumina film on a NiAl(1 1 0) single crystal surface. To our knowledge, this represents the first infrared study of a well-ordered oxide film under UHV conditions. Very narrow signals are observed, reflecting its high degree of order. The energies of the most intense features correspond to three out of four LO frequencies of bulk γ-Al_2O_3. In addition, the high spectral resolution attained with both methods enabled new phonon features to be identified, raising the total number of observed modes to at least 14. Microscopic lattice dynamical calculations will be required for a structural assignment of the observed signals to vibrational modes of the thin film.

Metal particles were then prepared on the oxide surface by vapor deposition of Pd, Rh, Ir, V, and Al. Controlling the metal exposure and the substrate temperature, particles with sizes ranging from below ten atoms up to several thousand atoms were grown. The metal deposits induce a damping, a frequency shift, and a broadening of the most intense oxide phonon infrared band initially located at 871 cm^{-1}. Frequency shifts by up to 15 cm^{-1} were observed. Adsorbed CO and ethene lead to further changes of the phonon spectrum.

A substantial number of dielectric and microscopic phenomena could be responsible for the observed changes. Our data provide an indication as to their relative importance, which varies with the amount of material deposited.

At low metal exposures, the intensity data for clean and CO-saturated particles point to the extent of perturbation at the metal–oxide interface determining the extent of phonon damping. This phenomenon is related to the reactivity of the admetals. At larger exposures, dielectric screening is likely to be more important. This may either occur via screening of the incoming infrared light by the metal or via dynamic dipoles of the oxide phonons inducing image dipoles in the metallic adlayer.

The phonon frequency increases according to $Pd < Ir \leqslant Rh < V \approx Al$ at low metal exposures. While Pd causes a red-shift, the other metals induce a blue-shift. Our frequency data, including those after CO-saturation, correlate with the d orbital or d band occupation of the admetals. As bourne out by an annealing experiment, also interface effects play a part. By contrast, mechanical detuning as a primary cause is ruled out. At higher metal exposures, a cross-over to a red-shift is observed for Ir, Rh, and V. A new phenomenon seems to govern the spectral behavior in this regime.

The phonon halfwidth rises with increasing metal–oxide contact area and increasing perturbation at the interface. Electron–phonon scattering is not the main cause of phonon broadening. It rather originates from phonon-defect scattering due to the heterogeneity introduced by the metal deposits.

Acknowledgements

For financial support of our work, we are grateful to a number of agencies: Deutsche Forschungsgemeinschaft (DFG), Bundesministerium für Bildung und Forschung (BMBF), and the Fonds der Chemischen Industrie. This work has also been supported by Synetix, a member of the

ICI group, through their Strategic Research Fund. M.F. and N.M. thank the Studienstiftung des deutschen Volkes for a fellowship. Finally, we would like to thank Professor T. Rahman for valuable discussions.

References

[1] R. Franchy, Surf. Sci. Rep. 38 (2000) 195, and references therein.
[2] K. Wolter, D. Scarano, J. Fritsch, H. Kuhlenbeck, A. Zecchina, H.-J. Freund, Chem. Phys. Lett. 320 (2000) 206.
[3] M. Wada, N. Tanaka, Jpn. J. Appl. Phys. 29 (1990) L1497.
[4] N. Tanaka, J. Mater. Sci. Technol. 13 (1997) 265.
[5] Th. Scherübl, L.K. Thomas, Fresenius J. Anal. Chem. 349 (1994) 216.
[6] T. Scherübl, L.K. Thomas, Fresenius J. Anal. Chem. 353 (1995) 589.
[7] Th. Scherübl, L.K. Thomas, Appl. Spectrosc. 51 (1997) 844.
[8] A.C. Diebold, D. Venables, Y. Chabal, D. Muller, M. Weldon, E. Garfunkel, Mater. Sci. Semicond. Process. 2 (1999) 103.
[9] K.T. Queeney, M.K. Weldon, J.P. Chang, Y.J. Chabal, A.B. Gurevich, J. Sapjeta, R.L. Opila, J. Appl. Phys. 87 (2000) 1322.
[10] G.A. Niklasson, C.G. Granqvist, J. Appl. Phys. 55 (1984) 3382.
[11] T.W. Noh, Y. Song, S.-I. Lee, J.R. Gaines, H.D. Park, E.R. Kreidler, Phys. Rev. B 33 (1991) 3793.
[12] M.F. MacMillan, R.P. Devaty, J.V. Mantese, Phys. Rev. B 43 (1991) 13838.
[13] E. Wäckelgård, J. Phys.: Condens. Matter 8 (1996) 5125.
[14] D.W. Berreman, Phys. Rev. 130 (1963) 2193.
[15] B. Harbecke, B. Heinz, P. Grosse, Appl. Phys. A 38 (1985) 263.
[16] R. Fuchs, K.L. Kliewer, W.J. Pardee, Phys. Rev. 150 (1966) 589.
[17] K.L. Kliewer, R. Fuchs, in: I. Prigogine, S.A. Rice (Eds.), Advances in Chemical Physics, vol. 27, Wiley, New York, 1974, p. 355.
[18] Ph. Lambin, P. Senet, A.A. Lucas, Phys. Rev. B 44 (1991) 6416.
[19] P. Brüesch, R. Kötz, H. Neff, L. Pietronero, Phys. Rev. B 29 (1984) 4691.
[20] C. Martinet, R.A.B. Devine, J. Appl. Phys. 77 (1995) 4343.
[21] T. Conard, J. Ghijsen, J.M. Vohs, P.A. Thiry, R. Caudano, R.L. Johnson, Surf. Sci. 265 (1992) 31.
[22] G. Thornton, S. Crook, Z. Chang, Surf. Sci. 415 (1998) 122.
[23] Z. Chang, G. Thornton, Surf. Sci. 459 (2000) 303.
[24] J.G. Chen, J.E. Crowell, J.T. Yates Jr., Surf. Sci. 185 (1987) 373.
[25] M.-H. Schaffner, F. Patthey, W.-D. Schneider, Surf. Sci. 417 (1998) 159.
[26] H. Ibach, D.L. Mills, Electron Energy Loss Spectroscopy and Surface Vibrations, Academic Press, New York, 1982.
[27] R.M. Jaeger, H. Kuhlenbeck, H.-J. Freund, M. Wuttig, W. Hoffmann, R. Franchy, H. Ibach, Surf. Sci. 259 (1991) 235.
[28] R.M. Jaeger, J. Libuda, M. Bäumer, K. Homann, H. Kuhlenbeck, H.-J. Freund, J. Electron Spectrosc. Relat. Phenom. 64/65 (1993) 217.
[29] M. Frank, M. Bäumer, R. Kühnemuth, H.-J. Freund, J. Vac. Sci. Technol. A 19 (2001) 1497.
[30] J. Libuda, F. Winkelmann, M. Bäumer, H.-J. Freund, Th. Bertrams, H. Neddermeyer, K. Müller, Surf. Sci. 318 (1994) 61.
[31] M. Heemeier, M. Frank, J. Libuda, K. Wolter, H. Kuhlenbeck, M. Bäumer, H.-J. Freund, Catal. Lett. 68 (2000) 19.
[32] A. Stierle, F. Renner, R. Streitel, H. Dosch, to be published.
[33] R.M. Jaeger, Dissertation, Ruhr-Universität Bochum, 1992.
[34] M.B. Lee, J.H. Lee, J. Korean Phys. Soc. 34 (1999) 502.
[35] M.B. Lee, J.H. Lee, B.G. Frederick, N.V. Richardson, Surf. Sci. 448 (2000) L207.
[36] M. Klimenkov, S. Nepijko, H. Kuhlenbeck, H.-J. Freund, Surf. Sci. 385 (1997) 66.
[37] M. Frank, M. Bäumer, Phys. Chem. Chem. Phys. 2 (2000) 3723.
[38] A. Stierle, V. Formoso, F. Comin, R. Franchy, Surf. Sci. 467 (2000) 85.
[39] R. Fuchs, K.L. Kliewer, Phys. Rev. 140 (1965) A2076.
[40] Ph. Lambin, J.P. Vigneron, A.A. Lucas, Phys. Rev. B 32 (1985) 8203.
[41] Y.T. Chu, J.B. Bates, C.W. White, G.C. Farlow, J. Appl. Phys. 64 (1998) 3727.
[42] R.L. Strong, B. Firey, F.W. de Wette, J.L. Erskine, Phys. Rev. B 26 (1982) 3483.
[43] M. Bäumer, H.-J. Freund, Prog. Surf. Sci. 61 (1999) 127.
[44] M. Bäumer, M. Frank, M. Heemeier, R. Kühnemuth, S. Stempel, H.-J. Freund, Surf. Sci. 454–456 (2000) 957.
[45] M. Frank, M. Bäumer, R. Kühnemuth, H.-J. Freund, J. Phys. Chem. B, in press (published on the Web on 16 August 2001).
[46] A.F. Hollemann, E. Wiberg, Lehrbuch der anorganischen Chemie, de Gruyter, Berlin, 1985.
[47] C.T. Campbell, Surf. Sci. Rep. 27 (1997) 1.
[48] M. Frank, R. Kühnemuth, M. Bäumer, H.-J. Freund, Surf. Sci. 427–428 (1999) 288.
[49] G. Fahsold, A. Bartel, O. Krauth, N. Magg, A. Pucci, Phys. Rev. B 61 (2000) 14108.
[50] P. Grosse, Mikrochim. Acta 2 (1991) 309.
[51] W.T. Petrie, J.M. Vohs, J. Chem. Phys. 101 (1994) 8098.
[52] L.H. Dubois, G.P. Schwartz, R.E. Camley, D.L. Mills, Phys. Rev. B 29 (1984) 3208.
[53] V. DeRenzi, R. Biagi, M.G. Betti, C. Mariani, Phys. Rev. B 49 (1994) 8198.
[54] Q. Guo, P.J. Møller, Surf. Sci. 340 (1995) L999.
[55] A.G. Thomas, P.J. Hardman, C.A. Muryn, H.S. Dhariwal, A.F. Prime, G. Thornton, E. Román, J.L. de Segovia, J. Chem. Soc. Faraday Trans. 91 (1995) 3569.

[56] J. Stubenrauch, J.M. Vohs, Catal. Lett. 47 (1997) 21.
[57] M.L. Colaianni, P.J. Chen, J.T. Yates Jr., Surf. Sci. 238 (1990) 13.
[58] J.G. Chen, M.L. Colaianni, W.H. Weinberg, J.T. Yates Jr., Surf. Sci. 279 (1992) 223.
[59] C.A. Ventrice Jr., D. Ehrlich, E.L. Garfunkel, B. Dillmann, D. Heskett, H.-J. Freund, Phys. Rev. B 46 (1992) 12892.
[60] F. Winkelmann, S. Wohlrab, J. Libuda, M. Bäumer, D. Cappus, M. Menges, K. Al-Shamery, H. Kuhlenbeck, H.-J. Freund, Surf. Sci. 307–309 (1994) 1148.
[61] F.M. Hoffmann, Surf. Sci. Rep. 3 (1983) 107.
[62] W. Kress, in: W. Kress, F.W. de Wette (Eds.), Surface Phonons, vol. 21, Springer, Berlin, 1991, p. 209.
[63] P.S. Bagus, G. Pacchioni, Surf. Sci. 236 (1990) 233.
[64] D.A. Papaconstantopoulos, Handbook of the Band Structure of Elemental Solids, Plenum Press, New York, 1986.
[65] M. Bäumer, M. Frank, J. Libuda, S. Stempel, H.-J. Freund, Surf. Sci. 391 (1997) 204.
[66] B.E. Nieuwenhuys, Surf. Sci. 105 (1981) 505.